HIGH-SPEED DOWNLINK COMMUNICATIONS WITH HUNDREDS Mbps FROM 50kg CLASS SMALL SATELLITES

Hirobumi Saito
Japan Aerospace Exploration Agency (JAXA), Institute of Space and Astronautical Science (ISAS), Japan,
koubun@isas.jaxa.jp

Naohiko Iwakiri[a] , Atsushi Tomiki[b], Takahide Mizuno[b], Hiromi Watanabe[a], Tomoya Fukami[a], Osamu Shigeta[c], Hitoshi Nunomura[c], Yasuaki Kanda[d] , Kaname Kojima[e], Takahiro Shinke[e], and Toshiki Kumazawa[f]

Recently small satellites start playing important roles in earth observation missions. It, however, is true that small satellites have drawbacks of sensor resolutions and down link data rate. As a solution to the latter drawback, we have developed novel communications system for 320Mbps down link with 16QAM for small satellites with 50kg class. We developed a new GaN HEMT X-band amplifier with high efficiency and small distortion, digital filter and pre-distortion processing with relatively low clock frequency in FPGAs, and small X-band on-board antennas. As ground segments, we are developing a compact S/X dual band ground antenna station and a high performance demodulator with turbo equalizer/decoder based on CCSDS high rate telemetry standard. These technologies will be demonstrated in 2014 by Japanese Hodoyoshi-4 satellite with 50 kg mass.

I. INTRODUCTION

Recently technologies of small satellites have been so matured that many earth observation missions are proposed. However, it is true that small satellite missions still have limitations of satellite functions compared to large satellites. Their main limitations are earth sensing capabilities as well as down link capabilities.

The purpose of this research is to develop a high-data-rate (typically 300Mbps) communication system which can be applicable to small satellites of 50 kg class. We will demonstrate our technologies on orbit using Japanese Hodoyoshi-4 Satellite launched in 2013[1].

Conventional large satellites are provided with several hundred Mbps down link system which consume high DC power of 100-200W. A small satellite with 50kg, however, can generate only as small as power of 100 W as total. A high data rate communication system could be allocated about 20W for 10 minutes communication pass. This is a power constraint for a high-data-rate communication system for small satellites.

We have been developing the communication subsystem both for the flight hardware as well as the ground system, paying attention to reduce the DC power and the mass of onboard instruments.

Section II devotes discussions on conventional systems and our novel system of high-data-rate down link for small satellites. Sec.III describes the development of novel GaN HEMT X-band power amplifiers and the pre-distortion processing, and test results of the engineering model of the onboard transmitter. Then the outlines of onboard antennas are described in Sec.IV. For ground segments, the receiving antenna and the high-data-rate demodulator are summarized in Sec. V. Sec.VI shows the simulation results to evaluate performances of this communication system as a whole. Sec. VII is the conclusions.

II. SYSTEM DESCRIPTION

II.I Conventional system and its problems

Recent earth observations such as optical imaging and SAR imaging by satellites require higher spatial resolutions and more image data. This means that the down link data volume should be increased. One way to increase the down link data volume is to use data relay satellites such as TDRSS of USA and DRTS of Japan. In this scheme, a long visible time compensates its relatively low bit rate for long communication range between a geo-synchronous orbit and a low earth orbit. However, the data relay satellite itself and its communication cost are expensive. Also the data relay link requires additional communication instruments and antennas for a space-space link.

Therefore, a cost-effective approach to increase the down link data volume seems to increase a data rate of downlink to an earth station which has a short visible time around 10 minutes. Figure 1 indicates down link data rates of low earth orbiting satellites as a function of satellite mass [3]. The figure shows that

[a] Tokyo University, Japan
[b] ISAS/JAXA, Japan
[c] AI Electronics Co. LTD., Japan
[d] Antenna Giken Co. LTD, Japan
[e] Addnics Corporation, Japan
[f] TOYO Corparatio, Japan

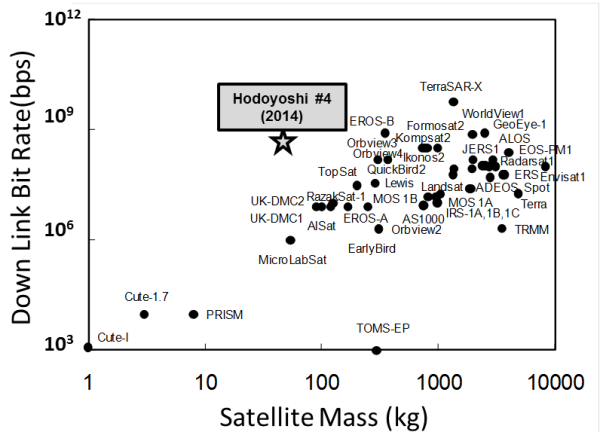

Fig.1 Down link bit rate vs. satellite mass for low earth orbit. ★denotes our novel technology.

down link data rates are proportional roughly to linear or square of satellite mass. This is because in general a down link with a high data rate requires high power consumption and large mass.

Conventional communication systems of large satellites have capability of hundreds Mbps through 1Gbps and in most cases they utilize X band (8025-8400MHz) for earth observation. The maximum bandwidth is 375MHz and in most cases a convolution coding with r=1/2 is applied. Therefore multi phase-shift-keying and amplitude-phase modulation are necessary to achieve higher bit rates than 300 Mbps.

These modulations, however, are sensitive to nonlinear distortion of RF power amplifiers. RF power amplifiers have to operate in linear region, which causes reduction of power efficiency. Also they require digital processing circuits with several hundred MHz clock. Space-qualified devices for

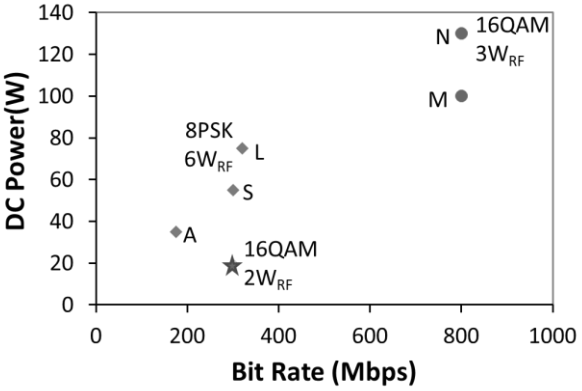

Fig.2 DC power consumption vs. data bit rate for onboard high-data-rate transmitter. ◆ and ● correspond to conventional transmitters with 8PSK and 16QAM, respectively. ★ denotes our novel transmitter with 16QAM. RF power levels are also indicated.

these purposes require high power consumption, high cost, and special care for ball grid array (BGA) devices. Figure 2 shows power consumptions as a function of data bit rate for onboard X-band transmitters with high data rates. Their power consumptions increase as the data bit rates increase with bandwidth-effective modulations.

Onboard antennas are medium or high gain antennas to satisfy their link budgets. The conventional earth observation satellites are so large that they are reluctant to manoeuvre to a ground station for communication link. Usually their antennas are mounted on movable gimbals, which also require high power consumption.

As sum of them, the conventional high-data-rate communication system of large satellite requires 100W or 200 W as a whole for DC power consumption.

Also ground stations for a high-data-rate down link have problems. As described in II.II link calculations indicate that ground antennas with several meter in diameter is enough for high-data-rate links. So we can share the ground antenna both for satellite control link (S-band) and high-data-rate link (X-band). Some of ground stations, however, are expensive facilities with a large diameter antenna for emergency command operations. Others with small antennas are dedicated antennas for X-band only. It is desired to develop a small, dual-band station with S-band up/down link for satellite operations as well as X-band data down link.

Since a ground station communicates with various satellites, a ground demodulator is required to have a clear interface with satellite. In most cases, conventional high-data-rate ground demodulators have been developed separately from developments of onboard transmitters. Manufacturers of ground station systems including parabolic antennas have also developed ground receivers. These situations have led to developer of ground demodulators to pay little attention to compensate or adapt imperfectness of onboard transmitter such as nonlinearity, an error angle of I-Q axes and frequency dependences.

Recently novel technical improvements of wireless communications have been emerged. It is desired to apply the "adaptive technology" to the high-data- rate demodulator for earth observation satellites.

II.II Developing system for small satellites

In Sec II.I, we described the conventional system and its problems of high-data-rate down link. In this section we propose several improvements for high-data-rate down link system as described in Fig.3, including a modulation scheme, an onboard RF amplifier and a transmitter, onboard small antennas, a

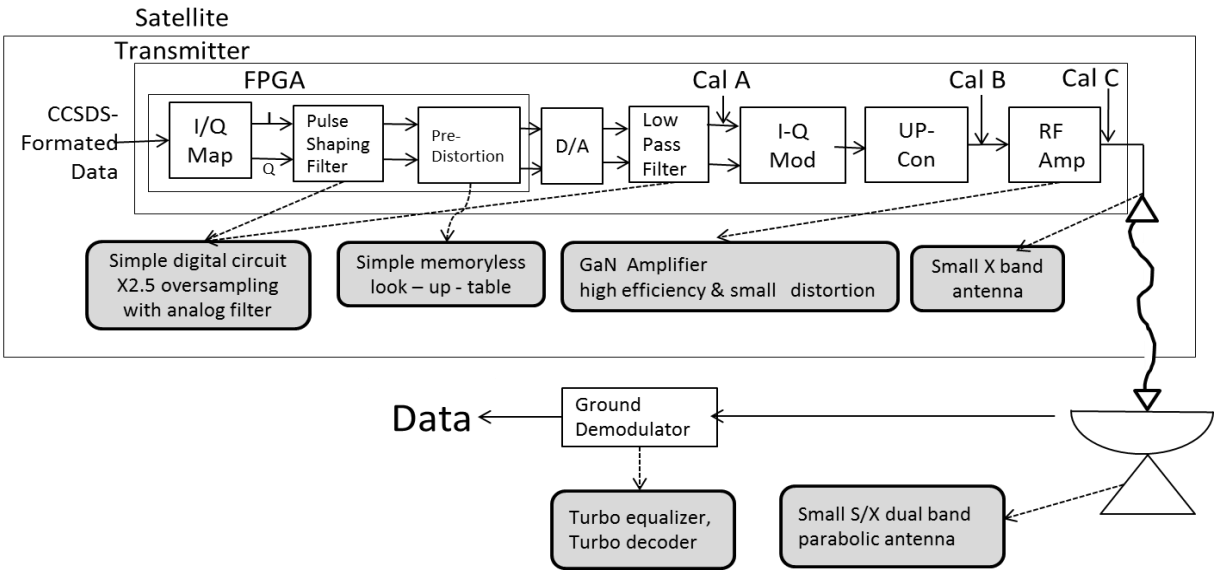

Fig.3 System block diagram of high-data-rate downlink. Several improvements are applied to satellite segment and ground segment.

Table 1: Performance of High-Data Rate Down Link

Instruments	Mass (g)	Power (W)	Remarks
On-board			
Transmitter	1330	18	16QAM, 348Mbps GaN Power Amp.
Antenna			
MGA	69	0	13.5 dBi
Iso-flux	150	0	5dBi(60°), -2dBi(0°)
Ground Station			
Antenna	3.8m Dia. S/X Cassegrain, 47.5dBi(X), 36dBi(S), Sys. Noise temp. 100K		
Demodulator	100Msps, (348-144Mbps), 16QAM, QPSK SCCC Turbo Equalizer CCSDS 131.2-B-1		

small S/X dual band ground station, and a high performance demodulator. Table 1 summarizes our novel communication system with high data rate for small satellites.

A. Modulation & protocol

Consultative Committee for Space Data Systems (CCSDS) 131.2-B-1 recommendation [3] is published to support a wide range of spectral efficiency values and rates for high-data-rate telemetry applications. Comprehensive coding and modulation schemes are defined as adaptive coding and modulation (ACM) modes including serially concatenated convolution turbo coding (SCCC) with various data rates using a punctured code and amplitude-phase shift keying (APSK).

QPSK modulations are applied to relatively low-data-rate links of ACM=1~6, where coding rates r are 0.36,0.43,0.52,0.61,0.70, and 0.81 for ACM=1~6.

At high-data-rate links of ACM=13~17, we replace 16APSK by 16QAM. This is because quadrature amplitude modulations (n-QAM) have more widely-spaced constellations than amplitude-phase shift keying (n-APSK) modulations. We can overcome nonlinearity of onboard transmitters as described in this paper. Then QAM becomes more promising than APSK. Coding rates r are 0.59, 0.66, 0.73, 0.80, and 0.87 for ACM=13~17.

Our symbol rate f_s is selected as 100Msps, taking into consideration the onboard digital hardware, frequency-band allocation of 100MHz, and the requirement for the data rates. The data rate R is given as $R = f_s\, r\, m$,where m is defined as m=2 for QPSK and m=4 for 16QAM. We can change the data rate R by changing the coding rate r or ACM.

B. Transmitter

The most important improvement of onboard instruments is to reduce their power consumption. We develop a small onboard transmitter for amplitude-phase modulation with low power consumption. We have developed three types of X-band power amplifies; GaAs field effect transistor (FET) amplifier of AB class, GaN high electron mobility transistor (HEMT)amplifier of AB class and of F class.

It is found that a GaN (HEMT) amplifier of AB class is the best among them and applied to this transmitter since it has high efficiency and low distortion. The nonlinearity of the RF power amplifier is compensated by memoryless pre-distortion. This

pre-distortion and a pulse shaping filtering are performed at field programmable gate arrays (FPGAs). The clock frequency of the FPGAs reduces to 125 MHz with assists of 2.5 oversampling technique and parallel processing, even though the symbol rate is 100 M symbol per second.

The mass is 1330g . DC power consumption is only 18 W, which is much smaller than other transmitters as indicated in Fig.2.

C. Onboard antenna

Two small onboard X-band antennas have been developed for this system, namely a medium gain antenna with 150g mass and an iso-flux antenna with 69g mass. The medium gain antenna (MGA) has 13.5dBi peak gain and 29° beam width. The MGA is body-mounted and is directed to a ground station by a coarse satellite manoeuvring with accuracy of about 5° . This operation achieves a high data rate, eliminating mechanical gimbals with considerable mass and power.

An iso-flux antenna is a wide-beam antenna suitable for an earth-pointing mode, whose peak gain is at peripheral region. For a moderate data rate, the iso-flux antenna is used to compensate variation of propagation losses during a visible pass when the satellite is in an earth pointing mode.

D. Ground system

We are developing a small, inexpensive parabolic antenna with 3.8m in diameter which has function of X-band down link in addition to S band up/down link for satellite operation. This ground station is at the Sagamihara campus of Institute of Space and Astronautical Sciences, JAXA and will be a main operation station for Hodoyoshi-4 satellite.

For this project, we are developing a high data rate demodulator with a turbo equalizer and CCSDS SCCC scheme.. As described in III, we measured the wide ranges of onboard RF power amplifiers. Their characteristics are applied for designing the ground demodulator. However, our demodulator is not specialized for specific types of transmitters but is adaptive for all transmitters. As described in VI, the demodulator compensates nonlinear distortion in I-Q constellation plane, and corrects the signals without any specific parameters of the onboard transmitter.

E. Communication link calculation

The performances of this high-data-rate downlink system shown in Fig.3 are simulated by the signal processing worksystem (SPW) [4]. The details will be described in VI.

The summary of the results are shown in VI (Fig.16). The required Eb/No (signal energy of one bit/noise spectrum density) are plotted as functions of ACM coding rate. The modulations are QPSK (ACM=1~6) and 16QAM (ACM=13~17). We apply to the flight model a GaN HEMT amplifier of AB class with pre-distortion.

Table 2 summarizes the communication link calculation and gives the received C/No (received power/noise spectrum density). The link margins can be calculated based on the received C/No at Table 2, the required Eb/No at Fig.16, and the data rate. Figure 4 indicates the link margin for GaN amplifier of AB class with on board pre-distortion as a function of data bit rate.

When the MGA is directed to a ground station by satellite attitude manoeuvring, a high-data-rate down

Table 2 Link Calculation

Items	Values	Comments
Satellite		
TX Power [dBW]	3.0	2W
TX Cable Loss [dB]	-1.0	
TX Ant Gain [dBi]	13.5	MGA
EIRP [dBW]	15.5	
Propagation		
Propagation Loss [dB]	-177.9	El=5° (2320km)
(altitude 600km)	-173.9	El=30°(1460km)
Rain & Atm. Loss [dB]	-2.1	incl. noise
Gnd Station		
RX Ant Gain [dBi]	47.5	3.8m diameter
Sys. Noise Temp [dBK]	20.0	100K
G/T [dB/K]	27.5	
Received C/No [dBHz]	91.6	El=5°
	95.6	El=30°

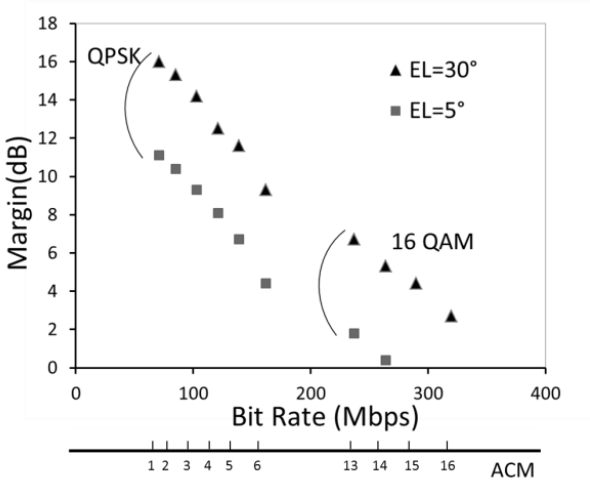

Fig.4 Link margin of high-data-rate down link as function of data bit rate or ACM number. Symbol rate is 100Msps, and elevation angle is 30° and 5° . Altitude is 600km and 13.5dBi MGA is applied. RF power amplifier is GaN HEMT of AB class with 26dBm input.

link with 320 Mbps is satisfied at a higher elevation t than 30° . Even when a satellite keeps earth pointing mode the iso-flux antenna maintains 104 Mbps during a pass.

III. TRANSMITTER

III.I RF power amplifiers

A GaAs FET device has been widely applied for X -band RF power amplifies. Recently a GaN HEMT device is considered as an amplifier of new generation. We developed three types of X- band power amplifiers, namely a GaAs FET amplifier of AB class, GaN HEMT amplifier of AB class, and a GaN HEMT amplifier of F class. The GaAs FET amplifier of AB class composes of FLM7785-4F (Sumitomo) which is internally matched with 1dB compression power of 36.5dBm. GaN HEMT amplifiers compose of the TriQuint TGF2023-01 bare chip with 0.25μm GaN production process and saturated output power of 37.5dBm. For the F class amplifier, the short circuit for the second harmonics and the bare chip are installed in a 3.2mm x.3.3mm microwave circuit board, and then the matching circuit for the fundamental frequency is externally installed. The AB class amplifier has a similar structure except that a through-line is installed in the 3.2mm x3.3mm circuit board.

We measured the output power (AM/AM characteristics), the power-added efficiency (PAE) and the phase shift (AM/PM characteristics) as functions of input power for three types of RF power amplifiers, since the nonlinearity of RF power amplifier is critical for amplitude-phase modulation. Figure 5 shows the results. Also Table 3 summarizes these parameters of three types of RF amplifiers. The GaAs amplifier has a relatively low power-added efficiency (PAE) (maximum 37%) and the moderate (10 °) phase shift at a high input power. The GaN HEMT amplifier of F class has a high power-added efficiency (maximum 60%) and a large (34°) phase shift at a high input power. As compared with these two, the GaN HEMT amplifier of AB class has promising characteristics for amplitude-phase modulation. Its power-added efficiency is relatively high (maximum 46%) and maintains high values at wide input range. The power-added efficiency at 3dB output back off point is still 36%. Also its phase shift is very small (less than 2°) even at a high input power. Note that this small phase shift makes GaN HEMT amplifier of AB class very promising for amplitude-phase modulations.

It is not yet understood why GaN-HEMT amplifiers of AB class show small nonlinear distortions, especially small phase shift, compared with GaAs-FET amplifier of AB class. A possible

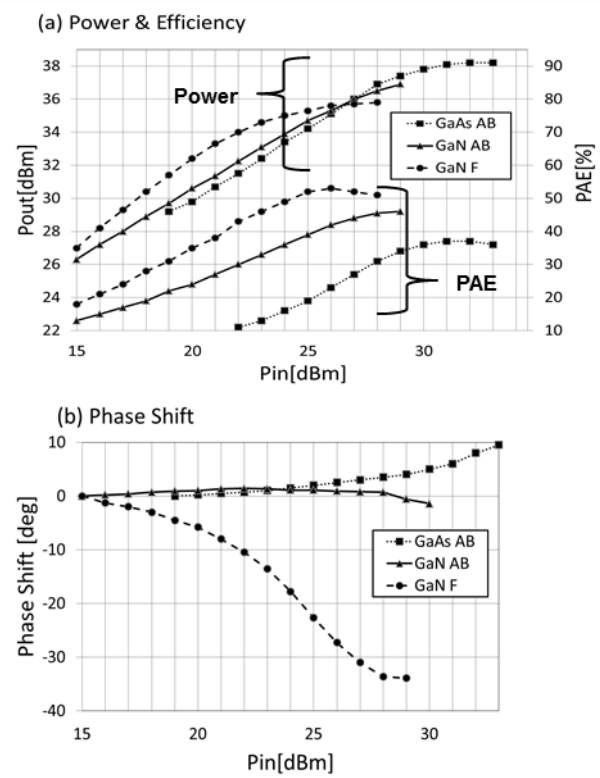

Fig.5 Comparison of three types of X-band RF power amplifiers. GaAs FET of AB class, GaN HEMT of AB class, and GaN HEMT of F class. (a) output power and power-added efficiency vs. input power. (b) phase shift vs. input power.

Table 3 Comparison of X-Band Power Amplifiers

Amplifier	GaAs AB	GaN AB	GaN F
Max. Power [dBm]	38	37	36
Max. Gain [dB]	10	11	12
Max. PAE [%]	37	46	60
PAE at 3dB OBO [%]	23	36	38
Max. Phase Shift [°]	10	-2	-34

reason may be the difference between their transistor structures. A FET has a structure in which thickness t_d of depletion region in the semiconductor is controlled by the gate voltage V_g. The relation between t_d and V_g is nonlinear. On the other hand, at a HEMT device, the charges Q_w at the quantum well region are controlled as a capacitor by the gate voltage V_g, resulting in variation of drain-source current. The relation between Q_w and V_g is linear. Another reason may be characteristics of drift velocity. Drift velocity of GaN keeps on increasing as electric field increases, while one of GaAs saturates and then decreases. These facts imply that a GaN HEMT amplifier show smaller nonlinearity.

Robustness against space environments is also important at selection of onboard amplifiers. Total ionization doze test was performed for the GaN amplifier of AB class at a Co 60 test facility. We gave the amplifier an ionization doze of 20krad in 1 hour without voltage supply since high-data-rate transmitters are in most cases activated for less than 2% of their mission period. The AM/AM, AM/PM characteristics and the efficiency do not change at all due to total ionization doze.

We measured temperature sensitivity of the GaN HEMT amplifiers of AB class. While ambient temperature varies between 31℃ and 46℃, the gain of the amplifier varies by 0.4dB for 12 dBm RF input and by 0.2 dB for 29 dBm RF input. Also the phase shift varies only by 0.5° . Characteristics of the GaN amplifier of AB class are very robust against total ionization doze as well as temperature variations. The GaN amplifier of AB class is suitable for onboard pre-distortion described in sec. III.III.

III.II Distortion by RF power amplifiers

The AM/AM and AM/PM characteristics of three RF power amplifiers give influences to performance of amplitude-phase modulation. We perform communication simulation with signal processing worksystem (SPW) [4], combined with the measured characteristics of the amplifiers.

The left two plots of Fig. 6 show measured characteristics of AM/AM and AM/PM for three frequencies with 100MHz bandwidth. Information data are modulated with 16 QAM. The symbol rate is 100 Msps. I and Q channel signals are sent to square-root-raised cosine filter with α =0.5. Then the

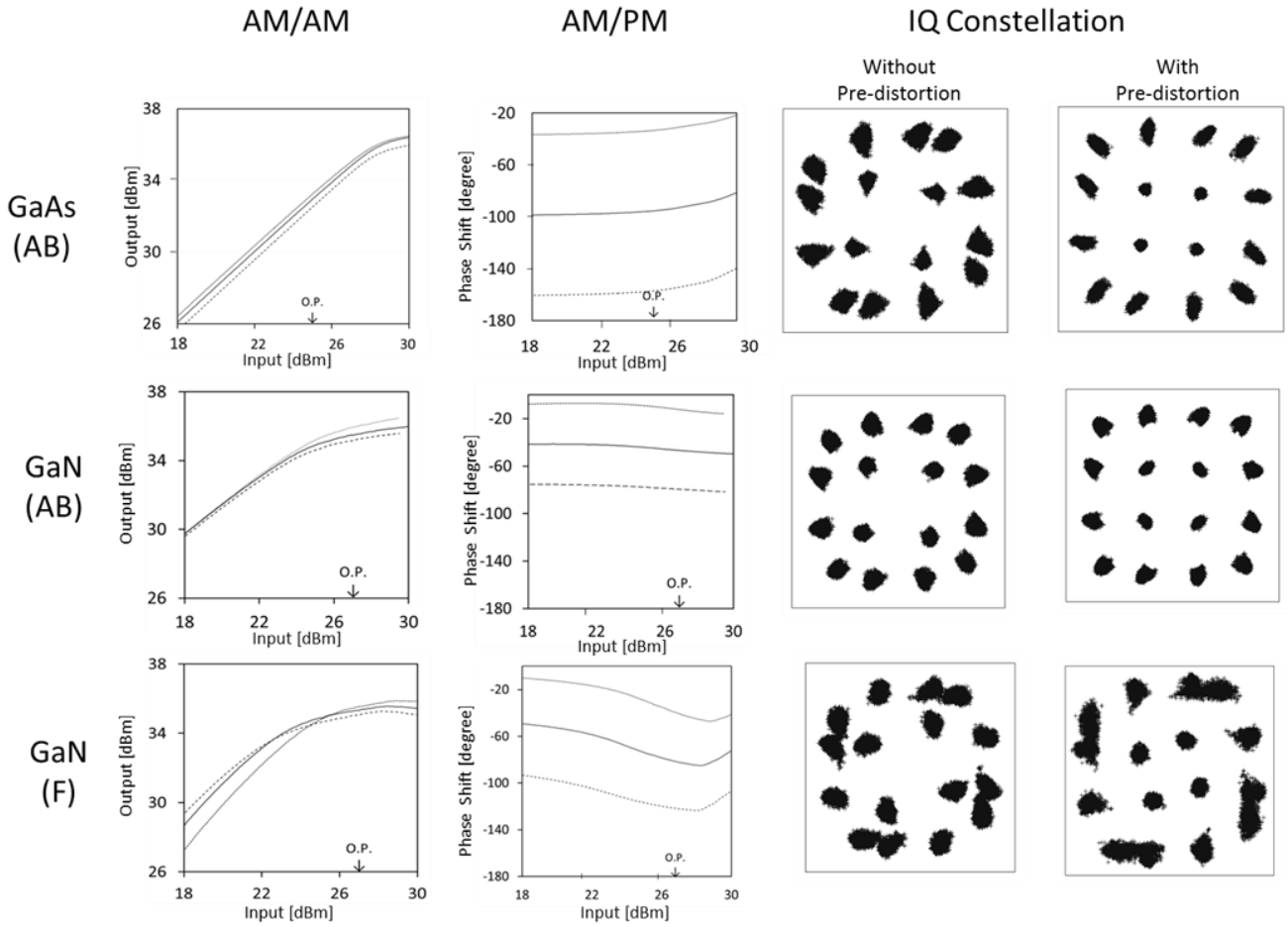

Fig.6 Nonlinearities of RF power amplifiers and their effects on IQ constellations for 16QAM. Amplifiers are GaAs FET amplifier of AB class (25dBm input), GaN HEMT amplifier of AB class (27dBm input), and GaN HEMT amplifier of F class (27dBm input). Nonlinearities are experimentally measured for 100MHz frequency bandwidth in terms of amplitude (AM/AM) and phase (AM/PM) characteristics. Thin line: 8150 MHz, thick line: 8200MHz, dotted line: 8250MHz. IQ constellations without pre-distortion and with memoryless pre-distortion are obtained by SPW simulation. Operating points (input power level) of amplifiers are shown by O.P.

digital-to-analogue converted signals are input to a RF power amplifier. We measured the AM/AM and AM/PM characteristics of RF power amplifiers at every 25MHz step and applied the measured results to the Poza–Sarkozy–Berger (PSB) model [5] including memory effects (frequency dependences). The operation points of the amplifiers set at input power level of 25dBm for GaAs FET amplifier of AB class and 27dBm for GaN HEMT amplifier of AB and F class, as marked with O.P. in the Fig.6. GaAs FET amplifier is a reference model. It has a relatively large phase shift and its operation point is selected with a large back-off.

The next ones to the most right plots of Fig. 6 are the simulation results of I-Q constellation demodulated at receiving side, where there are no pre-distortions. The I-Q constellations are distorted by the frequency dispersions as well as the nonlinearities of the amplifiers. Outer-squared 12 constellations are shifted inside nearly into a circle while inner-squared 4 constellations remain nearly squared suffering from a rotation. Each constellation cloud of a GaN HEMT amplifier of AB class is closer to a small circle and more uniformly separated than a GaN HEMT of F class and a GaAs HEMT amplifier of AB class since a GaN HEMT amplifier of AB class has a smaller phase shift (AM/PM). Outer clouds of the GaN HEMT amplifier of F class are connected with each other.

III.III Pre-distortion

We apply a digital pre-distortion technique [6,7] to obtain nearly linearized output signal with a high efficiency operation of the RF power amplifiers. As shown in Fig.3, this digital processing is performed in FPGAs after pulse shaping filtering.

Our symbol rate is limited to 100 Msps and the effective frequency bandwidth is about 100MHz, which is just 1.25% of the carrier frequency 8.16 GHz. The frequency dependences of AM/AM characteristics of Fig.6 (most left) are by less than 1dB while the nonlinearities are by 2-3 dB in terms of compression power level. The pre-distortion algorithm is memoryless pre-distortion with look-up-tables, neglecting frequency dependence of the system. I and Q channel signals passing through pulse-shaping filters are pre-distorted with the inverse characteristics of AM/AM and AM/PM of the RF power amplifier.

The simulation results with this pre-distortion are shown in the most right plots of Fig.6. The pre-distortions are especially effective to make uniform constellations between inner-squared 4 constellations and outer-squared 12 constellations. The size of each constellation cloud is determined by the linear and nonlinear dispersions (frequency dependence) of the amplifier. Clouds of outer-squared 12 constellations are larger than inner-squared 4 constellations due to nonlinear dispersion.

As a conclusion, we select the GaN HEMT amplifier of AB class with pre-distortion for the onboard power amplifier since it is provided with high efficiency, small phase-shift and compatibility for pre-distortion.

III. IV Design of transmitter

In this section, design of the onboard transmitter is described. Figure 3 in Sec. II.II includes the simplified block diagram of the transmitter. In the data handling instrument of the satellite, observation data are formatted in forms of adaptive coding and modulation ACM format of CCSDS 131.2-B-1 and then are sent to the transmitter.

The transmitter consists of a digital unit and an analogue unit. The digital unit is provided with two field-programmable gate arrays (FPGAs), Cyclon III, EP3C25, which is a low-power, flash type FPGA with 24,624 logic elements, 594kbits memory, 66 multipliers, and 4 PLLs. We selected a version with 148 pins plastic quad flat pack (PQFP), which is more robust for vibration and heat-cycle environments than a ball-grid array (BGA) version.

We confirmed that this FPGA is robust against 20 krad total ionization doze at Co 60 test facility. Another issue of onboard FPGAs is a single-event-upset (SEU) phenomenon. A SEU may induce an error of signal waveform, which is just a transient error. As a more serious error a SEU may destroy the configuration of circuits in FPGAs, which is stored in flash memories. A high-data-rate transmitter is operated only for short visible duration from a ground station. In prior to every operation, the circuits are configured from ROM memory which has SEU tolerance. Though the cross section and the threshold LET of Cyclon III, EP3C25 are unknown, available data of other re-configurable FPGAs imply a malfunction due to SEU during as short operation time as 10-15minutes is practically negligible. Cyclone III has an optional function of error detection of configuration data by CRC check. We may implement this function at the flight model. As a recovering operation against a possible configuration error, reboot function of FPGA circuits is implemented.

In the first FPGA out of two, data from the data recorder are mapped in I-Q constellation with 16 QAM or QPSK at 100 Msps. Then I and Q channel signals are pulse-shaping-filtered with a square-root-raised-cosine FIR filter. The sampling rate at the digital processing is selected to be 250 Msps, which is 2.5 over-sampling for 100 Msps signal. In order to apply this low sampling rate of 2.5 over-sampling, an

analogue low-pass filter is installed after the digital-to-analogue converter (Fig. 3) to eliminate the higher harmonics due to sampling. A parallel processing is instrumented in the FPGA and then the FPGA clock frequency reduces by half to 125 MHz. These points at design make it possible to select relatively low-clock- frequency and low-power FPGA with quad flat package (QFP).

In the second FPGA, a memoryless pre-distortion processing is installed with two parallel circuits for 125MHz clock operation. The FPGA stores a look-up-table that gives the nonlinear inverse-gains and inverse phase-shifts as functions of the input signal amplitudes. Complex signal of I and Q channel is multiplied by the complex correction values from the look-up-table.

The values in the table are determined by RF measurement of the transmitter described in III.V. Finally correction of error angle of I and Q channels is performed in the second FPGAs. Then the output from the second FPGA are sent to digital-to-analogue converters with 250 Msps clock. The analogue signals lead to the low-pass filter to eliminate the higher harmonics due to sampling.

The analogue I and Q signals are sent to the analogue unit. A PLL generates a stable local frequency f_o(=2.72GHz) at S-band. The I and Q channel signals modulate local signal f_o with a SiGe wideband direct modulator RFIC, Hittite HMC495. The modulated signal at f_o is mixed with $4f_o$ signals and is down-converted to a modulated signal at X-band ($3f_o$ =8.16GHz). Another frequency scheme would be a direct-modulation at X band. However, a voltage-controlled-oscillator (VCO) to generate X-band signal are vulnerable to leakage of modulated X-band signals with high power level. We did not select the direct modulation scheme. The modulated X-band signal is amplified by three stage driver-amplifiers and then is applied to the final power amplifier of GaN HEMT amplifier of AB class described in III.I-III.III.

As described above, the pre-distortion processing is performed in the transmitter. If the gain and the phase-shift of the transmitter varied in orbit, the pre-distortion would not work well. Therefore a calibration circuit is installed at the transmitter to measure the gain (AM/AM) and the phase shift (AM-PM) in orbit for various input levels and frequencies. Gain and phase detection ICs AD8302 (Analogue Devices) are selected to measure the gain/ phase of I-Q modulator and up-converter between the Cal A point and the Cal B point in Fig.3 as well as of the RF amplifiers between the Cal B point and Cal C point. We will measure the gain/phase in orbit and send to the ground through S-band downlink. If a finite variation of the AM/AM and AM/PM characteristics is recognized on the ground, we will renew the pre-distortion look-up-table through S-band uplink.

III.V Engineering model of transmitter

Design of the transmitter is verified through manufacturing and tests of an engineering model. The RF power amplifier of GaN HEMT amplifier of AB class is applied there as described in III. Figure 7 is a photograph of the engineering model. The mass and the DC power are 1330g and 18W, respectively. The engineering model consists of two trays. The upper tray contains the voltage convertors and the digital circuits with two FPGAs shown in the left part of the transmitter block in Fig.3. To transport heat from high-power RF circuits, the lower tray is devoted for the analogue and RF circuits shown in the right part of the transmitter block in Fig.3.

We developed an integrated measurement system of a high-data-rate transmitter as a whole. An arbitrary waveform generator (AWG) sends a sequence of test waveform to I and Q ports of a transmitter. An output RF signal from the transmitter is down-converted and stored by a digital oscilloscope. The recorded signal is numerically analysed to obtain all the characteristics of the transmitter such as I-Q inbalance, the angle between I, Q axes, frequency characteristics, the AM-AM & AM-PM characteristics, the I-Q constellation map, the error vector magnitude (EVM), and the bit error rate. The error angle of I and Q axes is found to be about 4° and the frequency dependence through the bandwidth of 100MHz is less than 1dB.

The time-average output RF power is about 33dBm as designed. This operation point of the RF power amplifier corresponds to about 24dBm input power level. We measured I-Q constellation maps

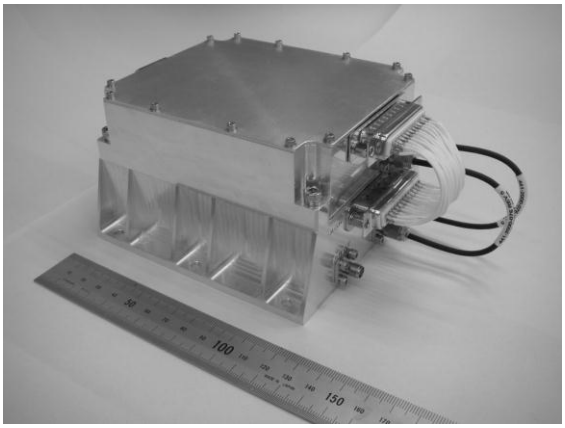

Fig.7 Photograph of engineering model of high-data-rate X-band 16QAM transmitter. Maximum data rate is 348 Mbps, RF output is 2W, DC power is 18W, and mass is 1330g and size is 120 x 120 x 73 mm^3.

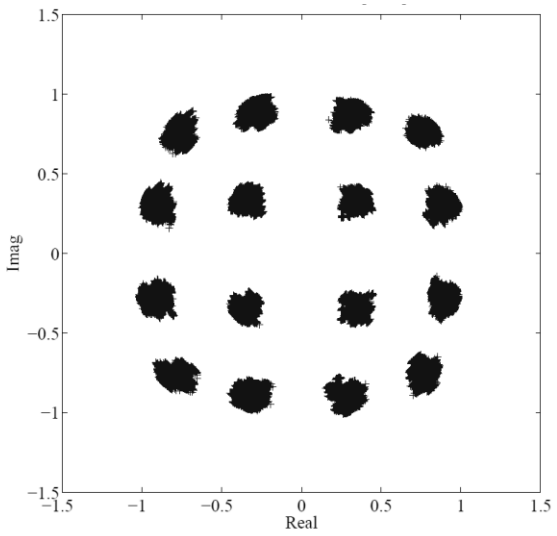

Fig.8 Measured IQ constellation of engineering model of transmitter with GaN HEMT amplifier of AB class. Symbol rate is 100Msps. RF output is 33dBm.

with 16QAM of 100Msps. The signal-to-noise ratio is very high and only imperfectness of the transmitter can be observed. The preliminary result is shown in Fig.8.

The pattern of the constellation in Fig.8 is qualitatively similar to the simulation result of GaN HEMT amplifier of AB class without pre-distortion in Fig.6, where input level is 27dBm. The input back-off of the measurement shown in Fig.8 is larger than the simulation shown in Fig.6. Nevertheless, the cloud size of the measurement is slightly larger than the simulation. The simulation does not include other nonlinearities and frequency dependences than ones of RF final power amplifier. These facts imply the imperfectness of other parts of the transmitter than the RF power amplifier seems not to be negligible. We have plan to carefully measure the characteristics of the transmitter as a whole and take into account them at the simulation and the pre-distortion design.

IV. ONBOARD ANTENNA

High-data-rate down link system for small satellites requires compact antennas with relatively high gain, which do not depend on mechanical gimbals. For this purpose we develop the compact medium gain antenna and the iso-flux antenna mounted on a satellite body.

IV.I Medium gain antenna

A medium gain antenna (MGA) mounted at a satellite-body is used to transmit high-data-rate down link. At this high-data-rate mode, the satellite attitude is manoeuvred so that the MGA is coarsely directed to a ground station within the MGA beam width. We

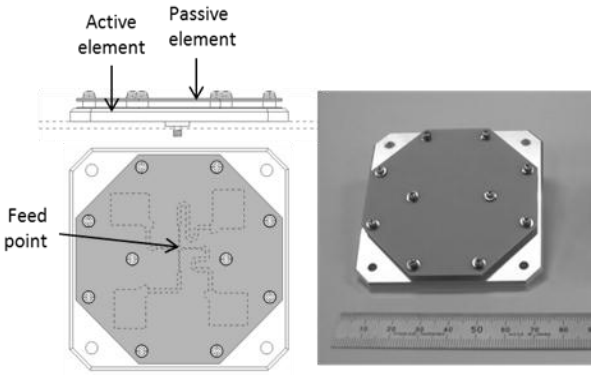

Fig.9 Structure and photograph of medium gain antenna with four active arrays and four passive arrays. Mass is 150g and size is 70 x 70 x 10mm^3.

select 2x2 arrays micro-strip antenna due to its compact size. The size is 70x70x10 mm^3 and the mass is only 69 g. Figure 9 is a structure and a photograph of the MGA.

The 2x2 arrays are aligned with spacing of $0.85\lambda_0$ to enhance its front gain. Passive elements are installed at 2mm above the active elements to aim a wider frequency band and a higher front gain. RF is fed from one feeding point and then is divided to four feeding circuits with each 90° phase difference for four active elements to generate a right-hand circular polarization wave. Computer simulation shows this antenna works for wide band from 7.3 to 8.9 GHz with VSWR<1.5 and the peak gain is expected to be 14.6dBi. The full width of 3dB level is estimated to be 29° .

IV.II Iso-flux antenna

An earth observation satellite, in most times, is in an earth-pointing attitude control mode. An iso-flux antenna is used to achieve a moderate data rate for as longer duration as possible when the satellite is continuously in an earth-pointing mode. In cases of 600km altitude orbits, distances between a satellite and a ground station varies from about 2,500km to 600km, as depicted in Fig.10. The propagation loss of the down link changes by almost 10dB. A satellite spends longer time at far positions from a ground station. An iso-flux antenna is a wide-beam antenna suitable for an earth-pointing mode, whose peak gain is at peripheral region of about $\theta=65^\circ$ to compensate the larger propagation loss, as indicated in Fig.12. Here θ is defined as an angle from the normal direction of the antenna surface.

Several types of iso-flux antennas have been proposed including quadrafilar helix antennas [8, 9], and aperture antennas with dielectric lenses. However, they do not satisfy the requirements for frequency

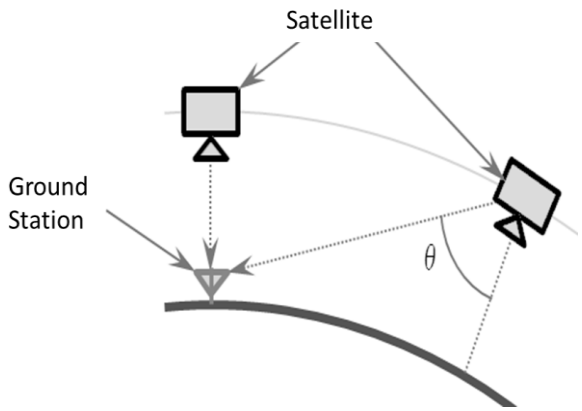

Fig.10 Iso-flux antenna with periphery - enhanced gain pattern compensates propagation loss at earth pointing mode.

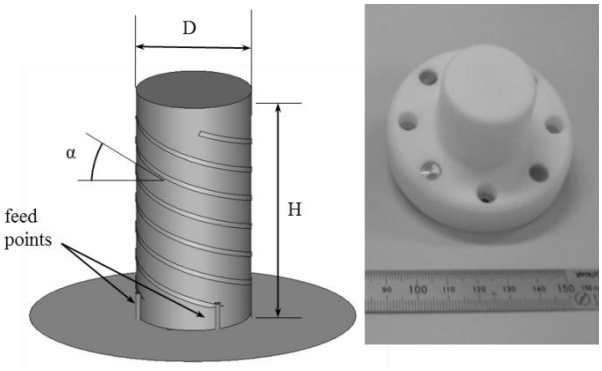

Fig.11 Structure and photograph of iso-flux antenna with qaudrafilar helix elements. Mass is 150g, α=20° , D=10mm, H=20mm.

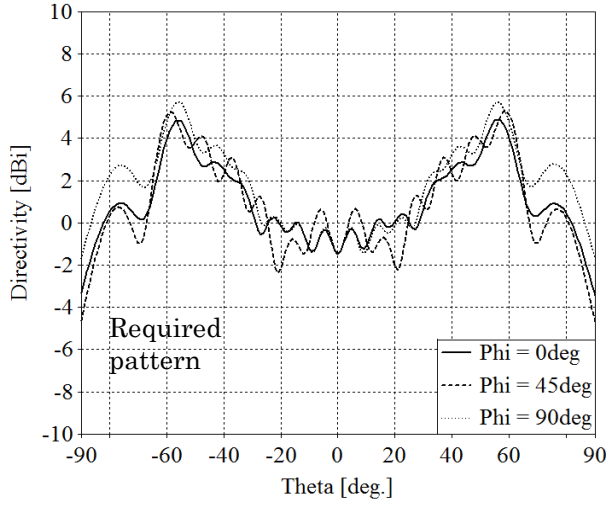

Fig.12 Simulation results of iso-flux antenna pattern with quadrafilar helix elements (α＝20°, D=10mm, H=20m). Theta is angle from antenna normal plane. Phi is azimuthal angle. Required gain pattern is also plotted for 600km altitude.

band, antenna gain pattern and small mass. We develop an X-band iso-flux antenna with quadrafilar helix elements, making compact feeding circuits with micro-strip lines. RF is fed to one feeding point for four feed circuits with each 90 ° phase difference and then sent to four helix elements. Figure 11 is a structure and a photograph of the iso-flux antenna. The mass is 150 g. A quadrafilar helix antenna can generate a circular polarization wave for a wider frequency band since its structure is almost azimuthally symmetrical. As the height of the helix increases, the beam is directed to periphery and the front gain deceases.

Figure 12 is the simulation result with pitch angle α=20° , diameter D=10mm, height H=20mm. Also the required antenna pattern to compensate the propagation loss for 600 km altitude is plotted.

V. GROUND SYSTEM

V.I Ground Antenna

Small satellites, in most cases, are operated with a small ground antenna. Frequency band for command and telemetry operation is typically S-band. It is desirable to provide the small parabolic antenna compactly with X-band down link capability.

We design and manufacture an S/X dual-band parabolic antenna with 3.8m in diameter. There are several antenna types for this purpose. The first is an S/X dual-band front feed parabolic antenna. It, however, is difficult to install S/X feeders with desirable patterns at the focal position of the parabola. The second is a parabolic antenna with a frequency selective reflector. It works as a Cassegrain antenna for X-band. There is a S-band feeder behind the frequency-selective sub-reflector which is transparent for S-band. However, frequency-selective surface with sharp curvature takes a cost and a risk to manufacture. The third is an S/X dual band Cassegrain antenna. It seems to be a reliable method although the S/X dual feeder structure becomes complicated.

Figure 13 is the structure of the main reflector, the S/X dual feeder, and the sub-reflector for Cassegrain antenna. The sub-reflector is an axis displaced ellipses with a ring focus. Incoming S/X-band waves are reflected at the main reflector and are focused at the focal ring. The sub-reflector is an elliptical surface and leads the incoming S/X-band waves to the system focus. The system focal position coincides the phase center of the S/X-band feeder. The S-band wave is collected by the circular corrugated horn antenna and is guided through the coaxial wave guide circuit. The X-band wave is collected by the dielectric rod and is propagated through the circular

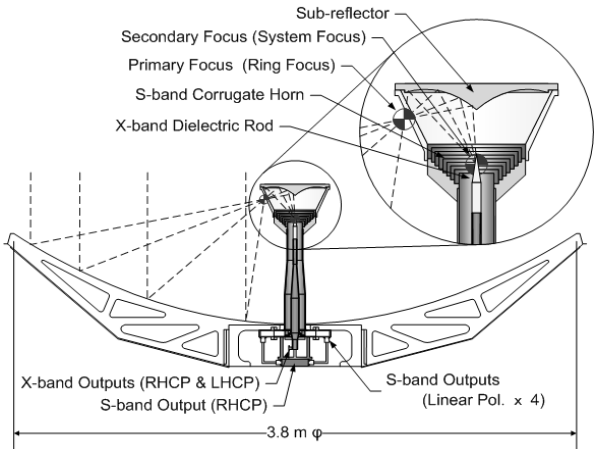

Fig.13 Structure of compact S/X dual band Cassegrain antenna with 3.8m diameter.

waveguide circuit installed inside the S-band coaxial circuit.

This S/X-dual band antenna of 3.8m diameter with reasonable cost will be installed at Sagamihara campus soon to be a main control antenna for Hodoyoshi-4 satellite.

V. II Receiver system

A X-band receiving signal from the small parabolic antenna is amplified by the low noise amplifier. Then the RF signal is down-converted to 1.2 GHz. A down converted complex signal with an oversampling factor of 4 (400Msps) is input into the receiver, as shown in Fig.14, which is the total block diagram of high-data-rate down link system[10] .

This input is first processed by a signal searcher to obtain the physical layer (PL) header timing by correlating the signals with the known frame marker (FM) symbols. The initial parameters, such as frequency and symbol phase offsets, are also estimated from the acquired timing, and then these parameters are passed to a frequency tracking loop (FTL) and time tracking loop (TTL). The FTL removes the residual Doppler frequency and carrier phase offset effects from the input signals based on the Costas loop[11]. On the other hand, the TTL provides the optimum symbol timing based on the Gardner loop[11], and then sends the suitable half-symbols r_n (operating at twice the modulation symbol rate) to the SCCC turbo equalizer.

A. Distortion compensator

Figure15 is the block diagram of turbo-equalizer [10]. The input half-symbols r_n is equalized at the symbol interference canceller (SIC) equalizer. Then the equalized symbol s_n is passed to the distortion compensator. 16-QAM modulation symbols induce serious nonlinear distortion as seen Fig.6 and 8, since sixteen signal points on two square constellations of different-size are sensitive to

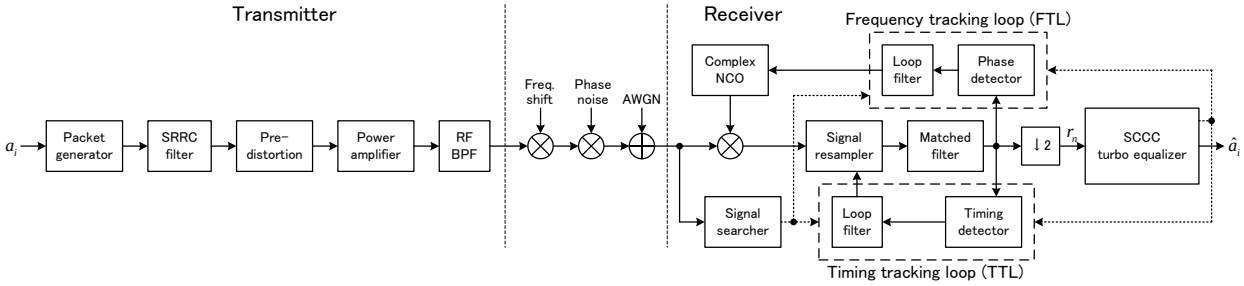

Fig.14 System block diagram of high-data-rate downlink including satellite segment (left) and ground station (right).

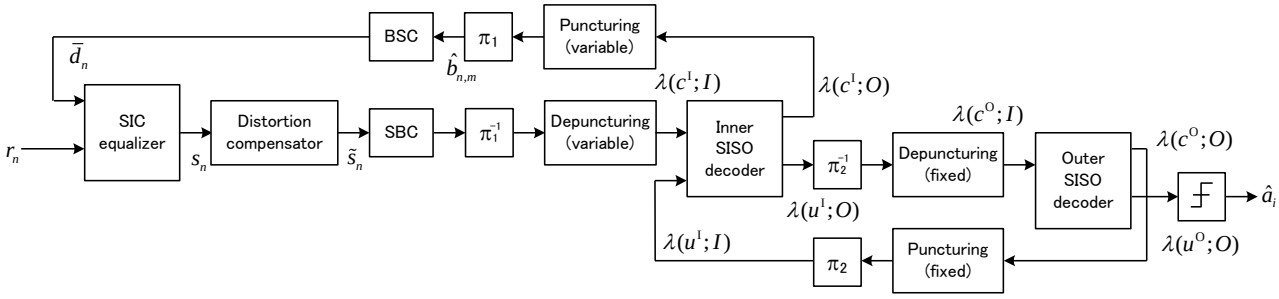

Fig.15 Block diagram of serially concatenated convolution turbo coding (SCCC) turbo equalizer at ground station. SIC: symbol interference canceller, SBC:symbol-binary converter , BSC:binary-symbol converter.

nonlinear distortion; thus, the distortion compensation techniques are required to mitigate the distortion at the ground demodulator, even though the pre-distortion at the satellite segment is performed as described in III.III.

The distortion compensation scheme consists of estimating each centroid of the 16 constellation points over the modulation symbols per code word section (CWS). It finds each error from the 16-QAM constellation points, correcting the error for each four points with the maximum and minimum Euclid distances from the origin of the constellation, respectively. Comparing the centroids of the transmitted and received signal constellations, the vector **u** connecting between the inner point and the outer point on-diagonal line is found to be different from the transmitted points owing to the nonlinear distortion. On the other hand the vector **v** connecting between the outer points or the inner points on the off-diagonal line is almost the same as the transmitted points because both edges of the off-diagonal vector **v** are at the same distance from the origin and suffer from the same nonlinear phase shift.

We can therefore apply a simple compensation process involving the rotation of **u** on the diagonal line for each quadrant.

B. Turbo equalizer

The SCCC turbo equalizer consists of two loops, as described in Fig15. The BER performance of the receiver strongly depends on the iteration procedure for the two loops. We heuristically find the procedure that provides the best BER performance.

The result is as follows: the two loops alternately update their output probability measures from the first to third iteration, and subsequently only the decoding loop updates the probability measures. In Fig. 15, the code symbols from the inner SISO decoder are fed back to the SIC equalizer, since feedback from the outer SISO decoder requires more complexity. The latter must be added an extra process, such as puncturing and interleaving for outer coding. Moreover, the obtained code symbols include more punctured symbols than those from the inner SISO decoder. The larger number of puncture symbols leads to a BER penalty as a result of the performance degradation of the SIC equalizer.

VI. SYSTEM SIMULATION

The high-data-rate downlink system combined with these newly developed satellite-segment and ground-segment was evaluated with a signal processing worksystem (SPW) [4].

A block diagram of the equivalent low pass model [5] for the high-data-rate communication system is shown in Fig. 14. On the transmitter side, a packet generator outputs modulated in-phase and quadrature (IQ) components, called modulation symbols. The modulation symbols are passed to a square-root raised cosine (SRRC) filter, followed by a digital pre-distortion block, RF power amplifier (PA) and an RF band pass filter (BPF). The RF power amplifiers are modelled with Poza–Sarkozy–Berger (PSB) [5] model including memory effects (frequency dependences), as described in III.II.

Then the RF signals suffer from Doppler frequency shift, phase noises and thermal noises as described in Fig.14. The blocks of the receiver side have already been explained in V.II.

We have carried out numerical simulation with SPW, paying attentions to SCCC turbo equalizer performances. Especially, a large number of iterations play an important role in improving the performance.

The summary of the results are shown in Fig.16. The required E_b/N_o (signal energy of one bit/noise spectrum density) are plotted as functions of ACM coding rate. The modulations are QPSK (ACM=1~6) and 16QAM (ACM=13~17). The broken line corresponds to an ideal linear channel with additive white Gaussian noise. Measured characteristics of the real RF power amplifiers shown in Fig.5 and 6 are applied to the simulations. The solid line and dotted line correspond to the case without and with pre-distortion for GaN HEMT of AB class with 26dBm input, respectively.

For QPSK modulations with higher coding rate (ACM=4~6) three curves coincide. This is because

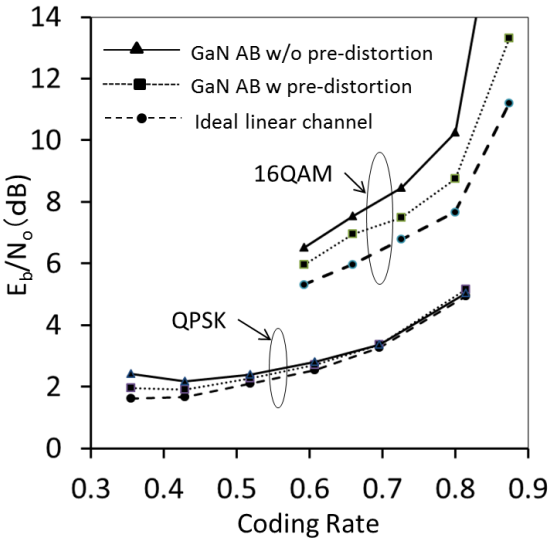

Fig.16 Simulation results of required E_b/N_o for 16QAM and QPSK as function of ACM coding rate. Broken line: ideal linear channel. Also E_b/N_o for GaN HEMT AB class amplifiers of 26 dBm input are shown. Solid line: without pre–distortion. Dotted line: with pre-distortion.

the QPSK modulation is a constant-envelop modulation and is robust against nonlinearity of RF amplifiers. However, for QPSK modulation with lower coding rate (ACM=1~3), three curves are slightly different, because a bit-synchronization error appears at a lower bit rate region.

For a fixed coding rate, 16QAM has two times higher data rate than QPSK modulation and consequently the required E_b/N_o of 16QAM is higher than the one of QPSK modulation. As coding rate increases, the coding performance degrades and the required E_b/N_o increases.

In order to reduce DC power of the transmitter, we have applied the highly-efficient GaN amplifier of AB class. The case without pre-distortion in Fig.16 indicates that the required Eb/No degrades by 1.5～3dB from the ideal linear channel due to its nonlinear distortion. The degradation becomes larger as the coding rate is higher due to decrease of coding performance.

We have introduced the onboard pre-distortion technique in order to mitigate the nonlinear distortion.

The case with pre-distortion in Fig.16 indicates that the required Eb/No improves by 0.5 ～ 2dB compared to the case without pre-distortion. Then the degradation from the ideal linear channel becomes as small as 1dB. This result indicates that the onboard pre-distortion technique for nonlinear RF power amplifiers is effective with assist of powerful performance of the turbo-decoder and equalizer .

VII. CONCLUSIONS

As a solution to drawbacks of small satellites for earth observation, we have developed novel communications system for 320Mbps down link with 16QAM for small satellites with 50kg class. We developed a new GaN HEMT X-band amplifier with high efficiency and small distortion, digital filter and pre-distortion processing with relatively low clock frequency in FPGAs, and small X-band on-board antennas. As ground segments, we are developing a compact S/X dual band ground antenna station and a high performance demodulator with turbo equalizer/decoder based on CCSDS high rate telemetry standard. These technologies will be demonstrated in 2014 by Japanese Hodoyoshi-4 satellite with 50 kg mass.

ACKONWLEGEMENTS

This research is partially granted by the Japan Society for the Promotion of Science (JSPS) through the “Funding Program for World – Leading Innovetive R&D on Science and Technology (FIRST Program),” initiated by the Councile for Science and Technoligy Policy (CSTP).

REFERENCE

[1] S. Nakasuka, “From Education to Practical Use of Nano-satellites - Japanese University Challenge towards Low Cost Space Utilization - ,” 8th IAA Symposium on Small Satellite for Earth Observation, Berlin, April, 2011

[2] CCSDS 131.2-B-1 “Flexible advanced coding and modulation scheme for high rate telemetry applications, Recommended Standard,” blue book, March. 2012

[3] M. Toyoshima, Y. Shoji, Y. Takayama and T. Maehata, “Log-likelihood coherent optical receiver –High-speed ADCless Architecture - ,” IEICE Technical report vol.110, No.46, pp.19-23, 2010.

[4] http://www.synopsys.com/systems/blockdesign/digitalsignalprocessing/pages/signalprocessing.aspx

[5] C. Jeruchim, P. Balaban, and K. S. Shanmugan, “Simulation of Communication Systems, “2nd ed., Kluwer Academic/Plenum Press, New York, 2000.

[6] Katz, A., “Linearization: Reducing Distortion in Power Amplifiers,” Microwave magazine, IEEE, Vol. 2, pp.37-47, 2001.

[7] E. Casini, R. De Gaudenzi and A. Ginesi, “DVB-S2 modem algorithms design and performance over typical satellite channels,” vol.22, pp.281-318, 2004.

[8] M. J. Josypenko, J. P. Casey, and S. M. Davis, “Quadrafilar Helical Antenna Array for Line-of-Sight Communications Above the Ocean Surface,” Undersea Warfare Electromagnetic Systems, NUWC-NPT Technical Report 11,820, 25 June 2007.

[9] J. Zackrisson, “SAAB Space X-Band Helix Antenna Family,” SAAB Document ID D-G-PRD-01309-SE, 2007.

[10] N. Iwakiri, A. Tomiki, T. Mizuno, H. Saito, and S. Nakasuka, “Performance analysis of SCCC turbo equalization with nonlinear satellite channel compensation techniques for nano/small satellite high-speed communication systems,” Proc. International Conference on Space, Aeronautical and Navigational Electronics 2011 (ICSANE 2011) , SANE-66, Bali, Indonesia, Oct. 2011.

[11] K. S. Andrews, A. Argueta, N. E. Lay, M. Lyubarev, E. H. Sigman, M. Srinivasan, and A. Tkacenko, “Reconfigurable wideband ground receiver hardware description and laboratory performance,” Interplanetary Network Progress Report, vol.42-18, pp. 1-22, Feb. 2010.